J. Fluid Mech. (1985), *vol.* 161, *pp.* 249–268
Printed in Great Britain

Influence of Bénard convection on solid–liquid interfaces

By C. DIETSCHE AND U. MÜLLER

Kernforschungszentrum Karlsruhe, Institut für Reaktorbauelemente, Postfach 3640, 7500 Karlsruhe 1, Federal Republic of Germany

(Received 25 January 1985 and in revised form 17 June 1985)

A laterally confined horizontal liquid layer is heated from below and cooled from above so that the single-component liquid is frozen in the upper part of the layer. When the imposed temperature difference is such that the Rayleigh number across the liquid is supercritical, there is Bénard convection in the liquid layer coupled with the dynamics of the solidification interface. Experimental results are presented for quasi-steady temperature variations at the horizontal boundaries. When the solidified layer is thick compared with the liquid layer a hysteresis loop is found for the heights of the liquid layer in a range of subcritical Rayleigh numbers. The interfacial corrugations exhibit a polygonal structure in this case. At Rayleigh numbers far above the critical value 'bimodal patterns' are observed with two distinct length-scales. Finally a stability chart is given for the various interfacial patterns observed.

1. Introduction

In many technical and natural processes free convection controls the freezing or melting of materials. This is the case, for example, for the freezing of ponds or of seawater (Farhadieh & Tankin 1975; Huppert & Turner 1978; Carey & Gebhart 1982; Diaz & Viscanta 1984) or for latent-heat energy storage employed in solar heating systems (Saitoh & Hirose 1982; Marshall & Dietsche 1982). Moreover, solidification processes and free-convective transport are key phenomena when crystals for semiconductor production are grown from a melt. Here the interaction between time-dependent convection and solidification can have a major effect on the quality of the crystal (Jakeman & Hurle 1972; Müller, Schmidt & Kyr 1980). A more detailed survey of related literature is given in the article by Davis, Müller & Dietsche (1984, hereinafter referred to as DMD). In that paper experiments and a weakly nonlinear instability theory of solidification influenced by Bénard convection were presented. The present work can be considered a continuation of the experimental work in DMD. Again, we wish to focus on systems in which thermal convection and corrugations of a liquid–solid interface are strongly coupled. We consider a horizontal layer of a single-component liquid, cyclohexane. The layer is heated from below and the boundary temperatures are adjusted so that the upper part is frozen and there is a solid–liquid interface. Depending on the Rayleigh number of the liquid, the heat in the liquid is transferred either by conduction only or by conduction and convection. The natural convection generally will occur in cellular form as is observed in Bénard convection. If the heat is transported uniformly by conduction only, the interface between the solid and liquid layer will be planar; however, it will become corrugated if natural convection occurs in the liquid. The situation is sketched in figure 1, and is the subject of our experimental investigation.

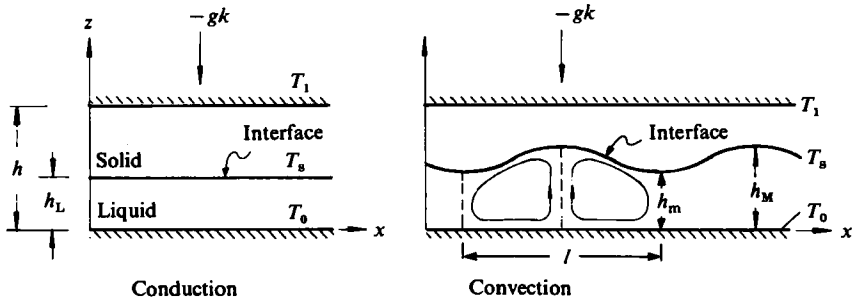

FIGURE 1. Schematic drawing of partially solidified liquid layer.

The most detailed analysis of the problem of pattern selection in single-component systems coupling Bénard convection and solidification is given in DMD. They point out that a deformable solid–liquid interface has a similar effect on the flow pattern in the liquid layer as a non-Boussinesq property of the liquid has in systems without solidification, i.e. the vertical symmetry of the Bénard system is broken in both cases. In particular the following results have been found: if the solid layer is very thin compared with the liquid layer and the interface is therefore only slightly deflected, the symmetry of the system is practically maintained. Thus convective roll patterns are established. However, with increasing thickness of the solid layer and increasing deformation of the interface, the asymmetry of the system becomes stronger and accordingly hexagonal convective patterns develop in the liquid layer resulting in a honeycomb-like structure of the interface. The change in the convection pattern is accompanied by a hysteresis loop of the liquid-layer height. Another hysteresis loop and a jump transition of the liquid height have been predicted at the onset of convection by DMD. So far, however, no experimental work is available to confirm these latter phenomena.

The main goal of the present investigation is to identify experimentally the hysteresis effect at the onset of convection. In addition, an exploration of other interfacial phenomena at fully developed convection is undertaken.

2. Apparatus and procedure

Compared with the previous test apparatus for an infinite layer described in DMD, a rectangular liquid-filled cavity of relatively narrow span is used here. The main reason for this is that visual observation of the solid–liquid interface and quantitative optical measurements are to be performed through transparent sidewalls. A cross-section of the test apparatus is sketched to scale in figure 2. The test volume has a height of 10.07 mm, a width of 20 mm and a length of 200 mm. It is confined between two copper blocks at the top and bottom respectively. The sidewalls consist of 2 mm thick Plexiglas. The distance between the polished surfaces of the copper blocks is fixed by placing polished Plexiglas spacers at the front sides of the test volume. The variance of the liquid height due to manufacturing tolerances is $\Delta h = \pm 0.01$ mm. The sealing of the Plexiglas sidewalls is done by the 'o'-ring material, Freudenberg Viton 70 FKM 598, at the top and bottom and by a special glue, Dow Corning 730 RTV, at both sides. At either side of the test volume, a 2 mm thick Plexiglas plate as well as a 4 mm thick glass plate enclose two 3 mm thick air slots. Even the largest vertical temperature differences realized in the experiments, about 20 °C, do not induce

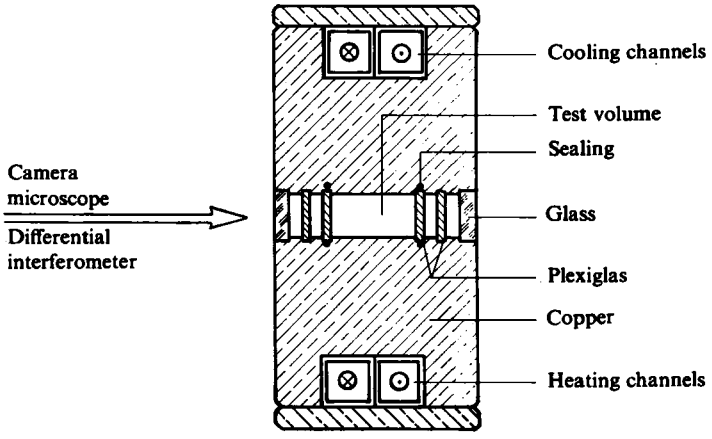

FIGURE 2. Cross-section of the experimental apparatus; height of the test volume 10.07 mm, width 20 mm, length 200 mm.

convection in the air slots (see Frick & Clever 1980). Therefore high thermal insulation of the test volume at the longer sidewalls of the cavity is assured.† For temperature control, countercurrent water channels are incorporated in the copper blocks. The supply of coolant is controlled by two high-precision thermostats of temperature variance $\Delta T = \pm 0.01$ °C. The whole test chamber, including the connecting pipes to the thermostats, is insulated against external temperature perturbations by styrofoam plates and rubber-foam hoses. Furthermore, the test chamber is placed in a temperature-controlled chamber, so that the air temperature around the test chamber can always be kept at the arithmetic mean value of the upper and lower boundary temperature of the test volume.

For measuring the temperatures at the horizontal boundaries of the test volume, four precision platinum resistance thermometers (Pt-100) are used. They are positioned two by two in the upper and lower copper blocks respectively, each 2 mm beneath the surface adjacent to the test volume. Each of the Pt-100 resistances is measured by a four-wire technique yielding an uncertainty in the temperature measurement of $\Delta T = \pm 0.02$ °C.

Cyclohexane (C_6H_{12}) is chosen as the test liquid since its physical properties are well known and there are no anomalies in them in the range -11 °C to $+9.4$ °C at which the experiments have been carried out. Moreover, cyclohexane is transparent in both the liquid and solid phases and has a fixed melting temperature. The latent heat of fusion Λ for this liquid is lower by a factor of 10 than that for water. Therefore steady-state conditions can be reached in reasonable time intervals. The Prandtl number is 17.6. The physical properties are listed in table 1. These properties are constant because the temperature T_0 at the heated bottom was fixed during the whole experiment at 3 °C above the melting temperature T_s. The ratio of the two thermal conductivities of the solid and liquid phases $\lambda^{(S)}/\lambda^{(L)}$ is given as a function of the temperature T_1 at the top, because this was varied over a range of 17.4 °C (for details see Dietsche 1984). The test substance used, cyclohexane, is the product 9666 pro

† For the design of the test apparatus the heat losses through the sidewalls of the cavity were calculated using the computer program HEATING (Turner & Siman-Tov 1971). The layout was fixed in such a way that the lateral heat losses were less than 5% of the total vertical heat-flow rate for all experimental conditions.

Kinematic viscosity	$\nu = 1.57 \times 10^{-6}$ m²/s
Thermal diffusivity	$\kappa = 8.9 \times 10^{-8}$ m²/s
Coefficient of thermal expansion	$\alpha = 1.17 \times 10^{-3}$ °C^{-1}
Melting temperature	$T_s = 6.4$ °C
Thermal conductivity of solid / Thermal conductivity of liquid	$\frac{\lambda^{(S)}}{\lambda^{(L)}} = 1.025 + 7.05 \times 10^{-3} \times T_2$ [°C]
Latent heat of fusion	$\Lambda = 31.3$ kJ/kg

TABLE 1. Physical properties of cyclohexane

analysis of Merck and contains less than 5‰ liquid and less than 10 p.p.m. solid impurities according to specification.†

Still photographs of the solid–liquid interface are taken under favourable lighting conditions. Liquid heights and wavelengths are measured using a Zeiss stereo microscope which is movable in three directions by a positioning table. The magnification factor of the microscope can be varied in 6 steps from 3.6× to 22×. The measurement of the lengths is accurate to within ±0.02 mm.

A differential interferometer is used for the visualization of density differences in the test substance. It is identical with the one used by Oertel & Bühler (1978). The differential interferometer generates lines of constant density differences in the direction of the beam separation. If the beam separation e is as small as in the present work ($e = 0.3$ mm), lines of constant density differences become lines of constant density gradients in the direction of beam separation. If the interferometer beams integrate the density differences only in one direction through the test section, as is the case in the present experimental set-up, quantitative evaluation of the fringe pattern is only possible for two-dimensional flows. The reason for this is that no information about the third dimension is provided. In our experiments fully two-dimensional flows could not be established. Therefore we confine ourselves to a qualitative evaluation of the interferograms.

The test procedure is conducted by varying the upper-boundary temperature T_1. The lower-boundary temperature T_0 is fixed throughout the experiments. Therefore the temperature difference across the liquid phase is always $T_0 - T_s = 3.0$ °C. The onset of convection is first investigated for an arrangement of 82% solid and 18% liquid material in the test volume. The temperature difference across the solid phase is then varied over a range of $T_s - T_1 = 14 \pm 3$ °C to study the onset and disappearance of convection in detail. During this procedure, changes in temperature are made in steps of 0.1 °C, where the rate of change is about 0.02 °C/min. When a stepwise change in the temperature of the upper boundary has been made the transient adjustment of the liquid height by solidification or melting at the interface lasts about 20 minutes. Since the time interval between two measuring points is at least 3 hours, and usually 8–12 hours, we can assume that the measurements have been performed under steady-state conditions. Furthermore, smooth interfaces without dendritic or 'feathering' structures are always generated since we deal with a single-component system and since the latent heat is extracted from or added to the solidification front quasi-steadily by conduction through the solid. According to Chalmers (1964) such interfaces tend to the configuration of the isothermal surfaces that would exist if no solidification or melting were taking place. After examining the onset and disappearance of

† These qualities assure that thermal-diffusion effects are negligible.

convection in detail, the temperature T_1 is then increased in steps of 0.5 °C and time intervals of 8 hours, yielding finally the pure Bénard case with $T_1 = T_s$. Then, by decreasing T_1 again, we investigate to what extent the observed phenomena at steady-state boundary conditions depend upon the particular path by which they are reached.

The experiments are described by introducing non-dimensional variables. It has been shown in DMD that the following quantity is relevant:

$$\frac{h-h_L}{h_L} = \frac{\lambda^{(S)}(T_s-T_1)}{\lambda^{(L)}(T_0-T_s)} \equiv A. \tag{2.1}$$

Here h is the total layer height, h_L is the liquid height for pure heat conduction, $\lambda^{(S)}$ and $\lambda^{(L)}$ are the thermal conductivities of the solid and the liquid phase respectively, and T_s-T_1 and T_0-T_s are the temperature differences across the solid and the liquid layer. A represents physically the ratio of the thickness of the solid layer to that of the liquid layer for the condition of pure heat conduction.

We also introduce the Rayleigh number R defined by

$$R = \frac{g\alpha(T_0-T_s)\,h_L^3}{\kappa^{(L)}\nu}, \tag{2.2}$$

where g is the gravitational acceleration, α the volume expansion coefficient, T_0-T_s the temperature difference across the liquid phase, ν the kinematic viscosity and $\kappa^{(L)}$ the thermal diffusivity of the liquid.

Note that, in contrast to the classical experiments of Bénard convection, the Rayleigh number is varied through changes in h_L and not through changes in the temperature difference T_0-T_s. Furthermore, by varying T_1 only, both the Rayleigh number and the parameter A are varied simultaneously.

As a measure for the spatial-periodicity lengthscale l we introduce a dimensionless wavenumber k by the relation

$$k = \frac{2\pi\bar{h}_L}{l}, \tag{2.3}$$

where $\bar{h}_L$ is the mean liquid height, i.e. the arithmetic-mean value of the local minima h_m and local maxima h_M of the liquid height (see figure 1). For steady-state heat conduction we have $\bar{h}_L = h_L$. We call l the wavelength of the spatial period in the solid–liquid interface. Owing to experimental scatter the distances between different local maxima and minima of the layer height are not exactly the same, nor are the values of the local maxima and minima. Therefore, mean values of the measured quantities $\bar{h}_M$, $\bar{h}_m$ and $\bar{l}$ are used in the graphs displaying the main experimental results (figures 4 and 15).

An analysis of the experimental errors has shown that the values of A are accurate to within $\pm 1\,\%$. The values for the Rayleigh number have a relative uncertainty of $\pm 1\,\%$ owing to the temperature measurement, and an absolute uncertainty of $\pm 7\,\%$. The wavenumber k is accurate to within $\pm 2\,\%$.

3. Results and discussion

3.1. *Onset of convection*

In figure 3 two photographs of the test volume are shown. The black stripes at the upper and lower end of each photograph represent the copper boundaries of the test volume. The thin line in figure 3(*a*) displays the planar solid–liquid interface. It

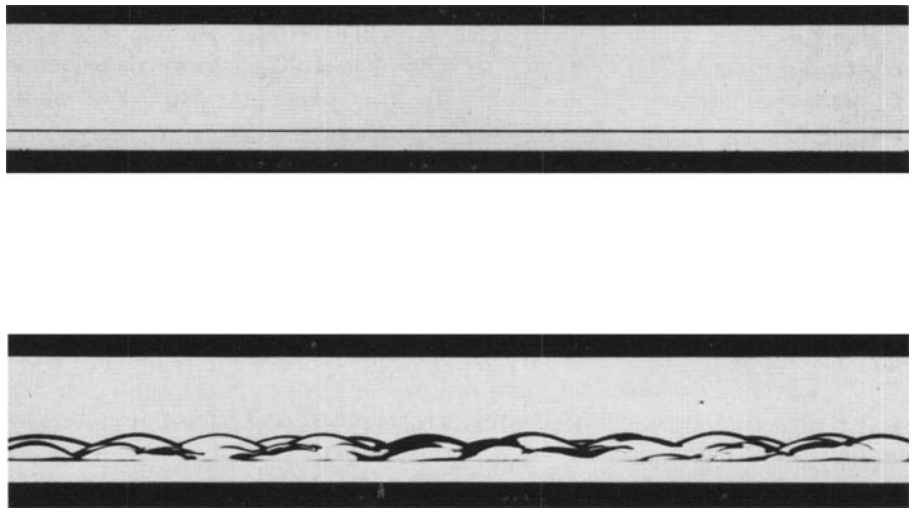

FIGURE 3. Steady-state patterns of the solid–liquid interface near the critical Rayleigh number: (a) $R = 1430$, $A = 4.61$; (b) $R = R_c = 1450$, $A = 4.58$.

separates the transparent solid phase in the upper part of the test volume from the transparent liquid phase in the lower part. Heat is transported by steady-state conduction only, so that the liquid height is equal to the heat-conduction height h_L. The value of the Rayleigh number is 1430. By increasing the Rayleigh number to a critical value $R_c = 1450$ convection sets in in the liquid phase and initiates a transient melting process. The final steady state of this transient process is shown in figure 3(*b*). The interface is no longer planar, but instead has a clearly three-dimensional structure. The local maxima h_M are more than 100 % larger than h_L. Since the liquid height at the lateral Plexiglas boundaries is controlled by heat conduction, it has the value h_L.

In figure 4 we show the phenomena at and near the critical Rayleigh number. The mean value of all measured local maxima of the liquid height h_M is divided by the total layer depth h and plotted as a function of the Rayleigh number R. The arrows indicate the path followed in the experiment. Starting from a value of 950, the Rayleigh number was increased quasi-steadily to its critical value of 1450. During this procedure the interface was found to be planar and the liquid height to be equal to h_L. At R_c convection set in and the dimensionless liquid height h_M/h increased by 117 % from 0.18 to 0.39. The experimental scatter of h_M/h indicated in figure 4 is due to the scanning with the microscope through the length of the test volume and evaluating single local maxima. At supercritical Rayleigh numbers no difference was found between the heights measured by increasing or decreasing the Rayleigh number. However, at subcritical Rayleigh numbers convection remained stable until a Rayleigh number of 1080 (−25 % subcritical) was reached.† At this point there was a transition to pure conduction, which is accompanied by a jump of the liquid height

† One of the reviewers pointed out that it may be useful to define a Rayleigh number R^* based on the mean liquid height $\frac{1}{2}(h_m + h_M)$. This can be done by using the measured values h_m and h_M displayed in figure 14. In this case the equilibrium state after onset of convection is characterized by a Rayleigh number $R^* = 9800$. When the temperature at the upper boundary is then reduced transition to pure heat conduction occurs at a Rayleigh number $R^* = 5500$, which is smaller by 40 % compared with the value of the equilibrium state after onset of convection.

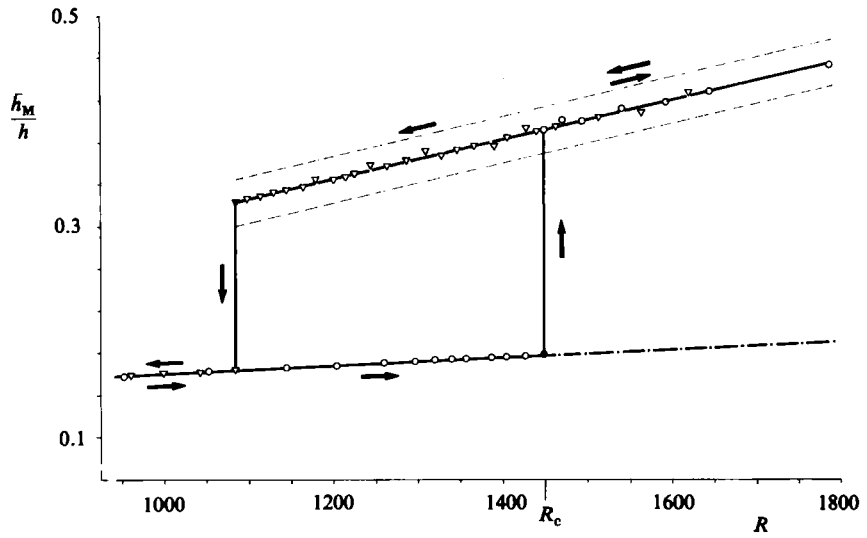

FIGURE 4. Hysteresis of the dimensionless maximum of the liquid height at the onset of convection. ○, steady state, $R\uparrow$; ●, melting; ▽, steady state, $R\downarrow$; ▼, freezing; —·—, unstable-heat-conduction height; = = = =, experimental scatter.

from 0.32 to 0.16. Thus, it is shown that the steady-state liquid height displays a strong hysteresis at the onset of convection. This is consistent with the analysis of DMD for an infinite layer. We consider the onset of convection, which takes place when the interface is planar. For values of A greater than 1, the linear theory gives a critical Rayleigh number of 1493. We measured a critical Rayleigh number of 1450, so that there is consistency of the above-described experiment with the linear theory to within 3%. A large sidewall influence on the value of R_c is not expected, since the aspect ratio $h_L{:}d$ is 1:10 at the onset of convection in our experiment (compare Frick & Clever 1980). DMD outline an analysis of weakly nonlinear interaction for a layer without sidewalls. They predict that the appearance of hexagonal convection is accompanied by a dynamic hysteresis behaviour and by jumping from one state to another. This is in good qualitative agreement with our experimental results. However, a quantitative comparison between the theory and our experiment is not possible because the experiment has been carried out at values of the parameter A of 4.5 whereas the above-cited analysis is valid only for small values of A.

Let us next discuss the experimental findings concerning the transients at the onset and disappearance of convection, indicated by vertical lines in figure 4. In figure 5 the normalized local maxima of the liquid height h_M/h at the onset of convection are displayed as a function of time. The total layer depth h (10.07 mm) and the thermal diffusion time $\tau_D = h^2/\kappa^{(L)}$ (19 min) are used as scales for length and time, respectively. Different measuring points are marked by figure numbers which identify photographs of the corresponding physical situations. The points marked with figure 3(a,b) represent the steady states that were discussed above. At time zero there was a step change in the Rayleigh number from 1430 to 1450. About 2.5 diffusion times later convection set in, which initiated a growing of the liquid height with an approximately exponential time behaviour. The three transient states, marked as figure 6(a–c), are shown in figure 6. Figure 6(a) shows the onset of convection. The critical wavenumber

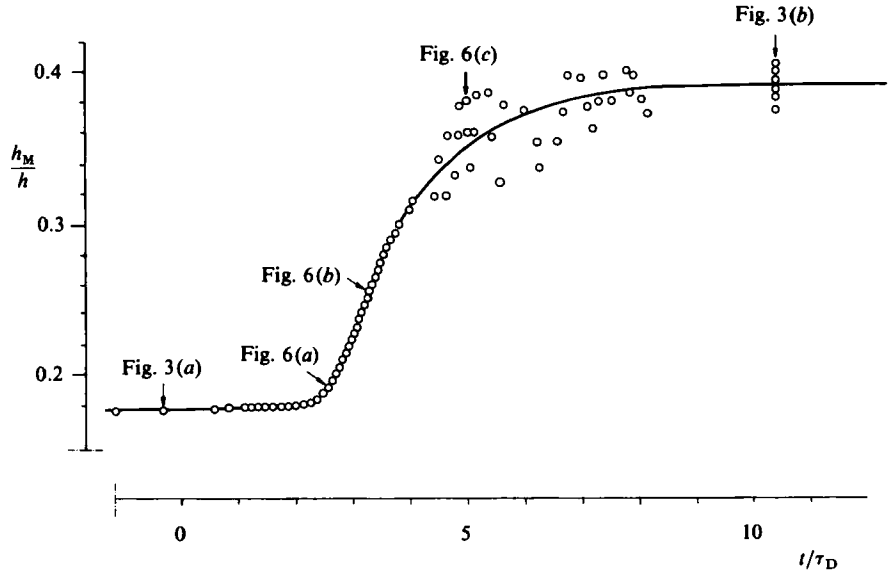

FIGURE 5. Time dependence of the dimensionless local maxima of the liquid height at the onset of convection.

measured is approximately 2.8, which compares well with the corresponding value of 2.82 according to a linear-stability theory (see DMD). In figure 6(*b*) it can be seen that the pattern of the interface has a very regular three-dimensional structure throughout the test volume. In figure 6(*c*) a rather irregular pattern is shown, exhibiting a greater scatter in h_M.

DMD showed that hexagonal patterns are expected when sidewalls are distant. The conditions of figure 6(*b*) closely resemble this situation since h_M is small compared to the width of the chamber. Figure 6(*c*) shows a much less regular pattern since the liquid layer has thickened by a factor of two and so the sidewalls have a greater influence. We found that sidewall effects become important when the aspect ratio based on the mean liquid height exceeds about $\frac{1}{8}$.

When a step change in the Rayleigh number from 1100 to 1080 was introduced, the convection did not disappear simultaneously throughout the whole layer. Instead a reduction of the liquid height and the intensity of the convection occurred first in the middle of the chamber and at the endwalls. Then the two remaining convecting zones of about 6 cm length each contracted in the horizontal direction, and finally the liquid heights were reduced in the vertical direction to h_L. Thus, no representative transient time dependence of the liquid height for the whole layer can be given. This behaviour was not expected because no inhomogeneity of the test volume could be identified either at the onset of convection or at any other time during the measuring procedure. Apparently even the slightest and, as in this case, immeasurably small inhomogeneities of the test volume can cause the behaviour described above. The total time needed for the transient freezing process was about 12 hours, 4 times longer than needed for the melting process at R_c. Consider that during the melting process at R_c the latent heat of fusion has to be transported through the liquid layer of thickness 2–4 mm, whereas during the freezing process at $R = 1080$ the latent heat of fusion has to be transported through the solid layer of thickness 6–8 mm. The ratio of the diffusion times of the two layers of mean thicknesses 6 and 3 mm is about 4.

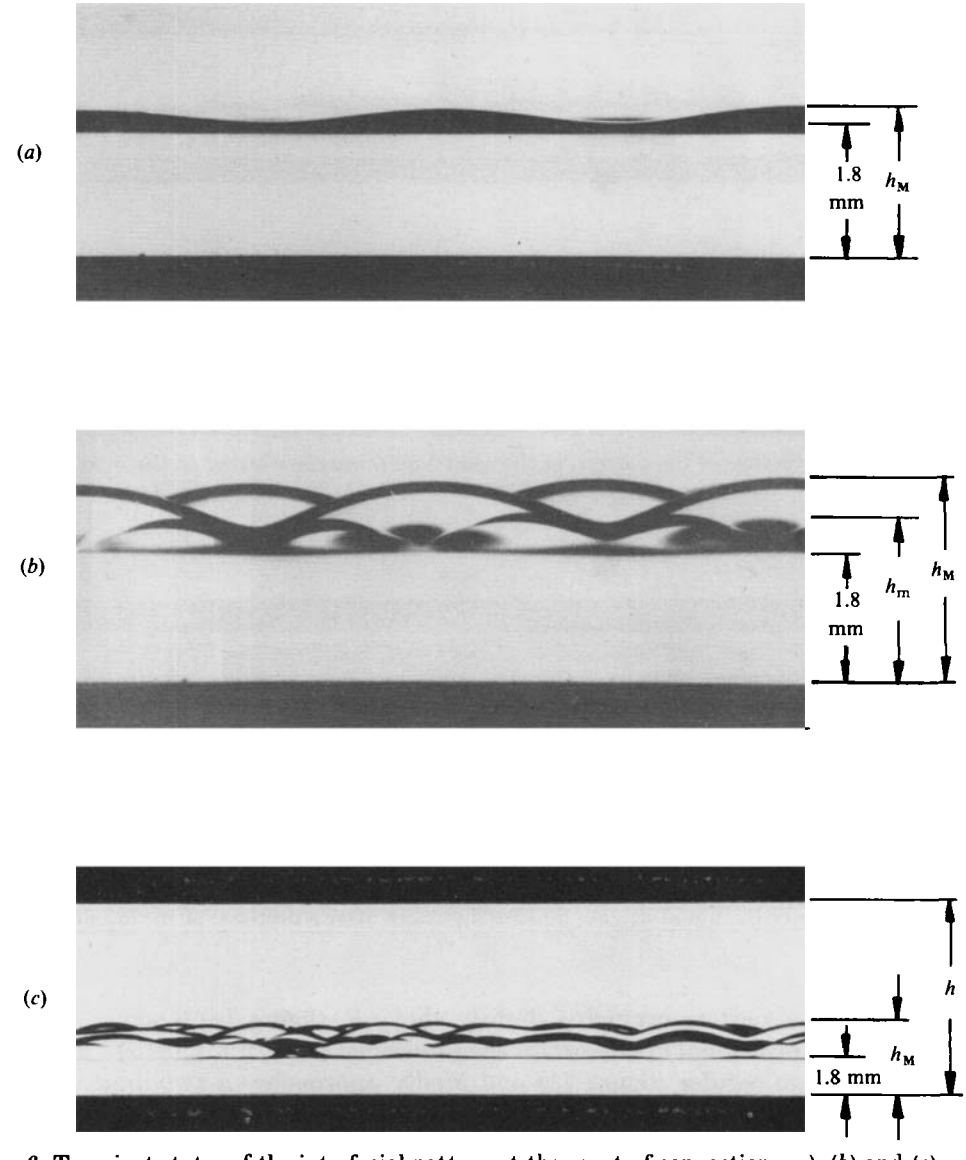

FIGURE 6. Transient states of the interfacial pattern at the onset of convection; (*a*), (*b*) and (*c*) refer to figure 5 above; note the change in scale from (*b*) to (*c*).

We therefore suggest that the difference in the time intervals between the melting and freezing processes considered above is due to the difference in the thicknesses of the layers.

3.2. *Fully developed convection*

We report next observations related to fully developed convection at supercritical Rayleigh numbers and discuss the related physical mechanisms.

When the experiment described in the preceding section is continued by increasing the temperature T_1 at the upper boundary the height of the liquid layer also increases. This leads to a change in the pattern in the solid–liquid interface (figure 7). Whereas

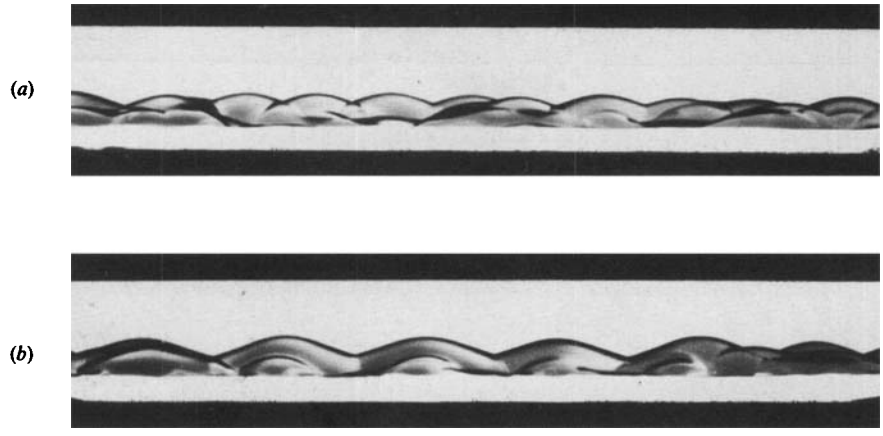

FIGURE 7. Change of the pattern of the solid–liquid interface owing to the influence of the lateral walls: (a) $R = 1800$, $A = 4.23$; (b) $R = 2100$, $A = 3.94$.

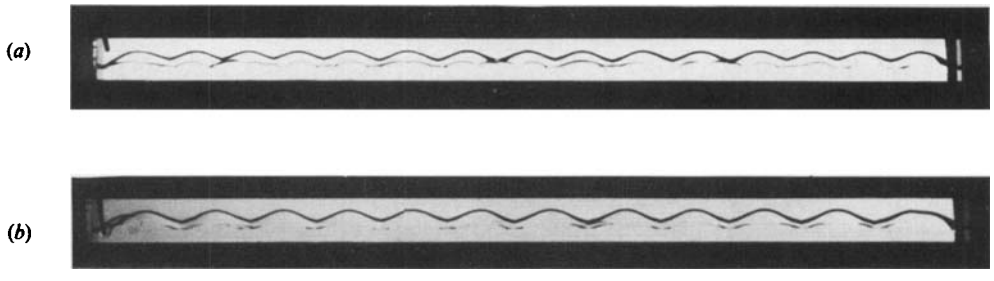

FIGURE 8. Different steady roll pattern at $R = 5100$ and $A = 2.67$: (a) 15-roll pattern after an increase of the liquid height; (b) 12-roll pattern after a decrease of the liquid height.

the interfacial pattern occurring slightly above R_c (figure 7a) is somewhat irregular and three-dimensional in character, the interfacial pattern for greater liquid heights becomes more regular (figure 7b) and finally approaches a two-dimensional form, which we shall hereafter call 'roll pattern'. The term 'roll pattern' suggests that the convection in the liquid layer has the approximate form of rolls whose axes are parallel to each other and to the shorter vertical side of the test volume. Such flow configurations have been predicted and observed for Bénard convection in small rectangular boxes (Davis 1967; Stork & Müller 1972). The cross-sectional aspect ratio of the liquid layer (i.e. the ratio of the mean liquid height to the layer depth) is about 1:4 when this reorientation of the interfacial pattern occurs. Thus we ascribe the reorientation of the interfacial pattern to the increasing influence of sidewalls of narrow span on the flow pattern with increasing liquid height. We mentioned in the previous section that a weak influence of the lateral walls on the interfacial pattern could be seen near R_c at an aspect ratio of about 1:8. There we find an irregular three-dimensional interfacial pattern instead of a regular hexagonal pattern as predicted by DMD for an infinite layer. This is also true for all aspect ratios between 1:8 and 1:4.

The roll pattern proves to be non-unique for certain supercritical but fixed

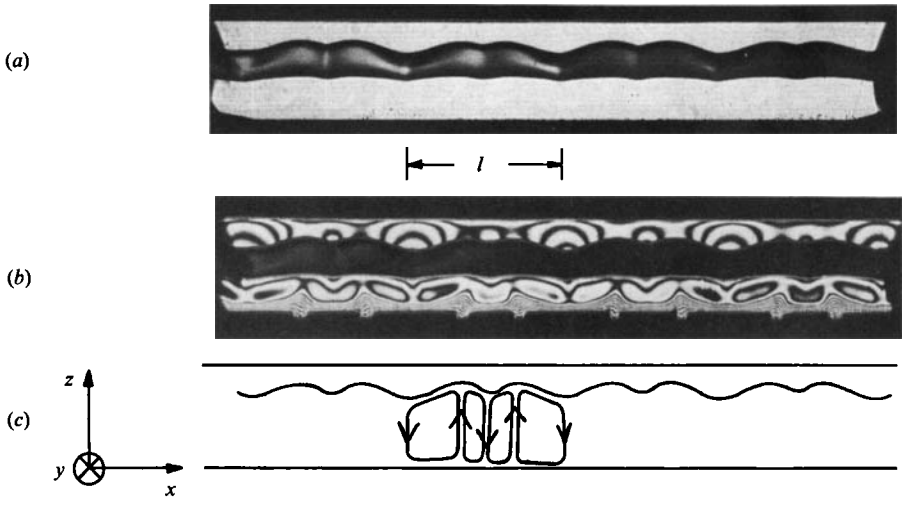

FIGURE 9. Bimodal pattern at $R = 10700$ and $A = 1.86$: (*a*) photograph; (*b*) differential interferogram of vertical beam splitting $e = 0.3$ mm; (*c*) streamlines.

boundary conditions. We find different steady-state interfacial patterns depending on the way in which the corresponding thermal boundary conditions are established. In figure 8(*a*), a steady state is shown, reached by increasing the temperature T_1, i.e. by increasing the liquid height. In this case 15 'rolls' are found in the test volume. However 12 'rolls' appear when the same boundary conditions as in figure 8(*a*) are established by decreasing the temperature T_1 (figure 8*b*). As an explanation for this non-uniqueness of the pattern, we propose that the wavelength of the particular convective roll pattern becomes 'frozen' by the interfacial corrugations. This means that, when the liquid-layer height is increased by melting the solid layer, the existing shape of the interface enforces the convection to maintain its wavelength. This is, however, smaller than the natural wavelength of the roll pattern for a corresponding (increased) layer height and fixed plane boundaries. A similar argument holds for the case where the liquid-layer height is decreased by 'freezing' from above.

For even greater liquid heights, i.e. higher values of the Rayleigh number, a new interfacial pattern is observed. This is shown in figure 9(*a*). Here two different horizontal lengthscales can be recognized from the shape of the solid–liquid interface.

We next consider figure 9(*b*). This displays a differential interferogram of vertical beam splitting $e = 0.3$ mm, and shows lines of constant vertical density gradients. The interferogram is evaluated qualitatively. (A quantitative evaluation was omitted because the three-dimensionally distorted interface, reproduced as a dark shadow, hides a major part of the test volume and because an easy quantitative evaluation would require the velocity and temperature fields to be purely two-dimensional.)

We see that in the interferogram the lower boundary of the liquid region features small protrusions in a regular arrangement. This phenomenon is due to light deflection in a variable-refractive-index field. The angle of light deflection towards the colder part of the test cell is proportional to the mean vertical temperature gradient $(1/d)\int_0^d (\partial T/\partial z)\,\mathrm{d}y$ (where d is the depth of the test volume) at the lower boundary (Hauf & Grigull 1970; Koster 1983; coordinate system as indicated in figure 9). We conclude, therefore, that near the protrusions there is a lower mean vertical temperature gradient than in the dark regions between the protrusions. In

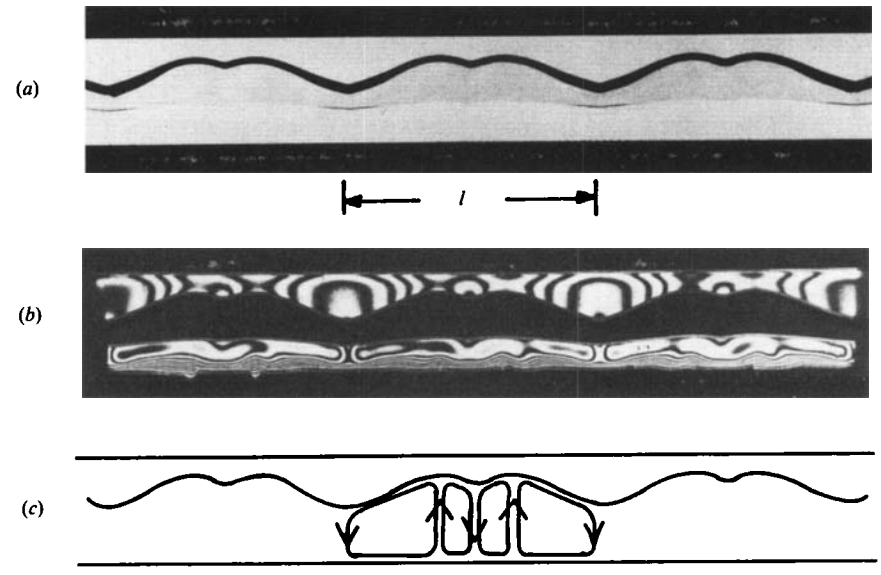

FIGURE 10. Bimodal pattern at $R = 10700$ and $A = 1.86$: (*a*) photograph; (*b*) differential interferogram of vertical beam splitting $e = 0.3$ mm; (*c*) streamlines.

analogy to the Bénard convection (see Oertel & Bühler 1978) we conclude that, near the protrusions, zones of locally lower temperature gradients exist where predominantly upward motion occurs, and that between them downward motion prevails. Since the aforementioned effect of light deflection is an integral effect with respect to the y-direction, the above conclusions are only valid in an integral mean. Similar qualitative conclusions can be drawn from the fringe pattern of the interferogram. The high density of fringes near the bottom of the layer indicates that there is a much stronger change in the vertical temperature gradient at the horizontal boundary than in the mean part of the liquid, i.e. there is a thermal boundary layer along the lower boundary of the liquid. However, the fringes along the lower boundary have peaks just above the protrusions. This indicates that in the vicinity of the protrusions the thermal boundary layer is thicker, and thus the vertical temperature gradient smaller, than in the longitudinal average. This confirms our conclusion that near the location of the protrusions we find warm upward motion. We also recognize in figure 9(*b*) that the warm upward flow occurs in zones where the liquid heights have their maxima. Thus the interface reflects the upward (and downward) motion in the liquid and we suggest that the fluid flow is basically of the form shown in figure 9(*c*), i.e. a transversal roll pattern. There is warm upstream motion in zones where the liquid height has its maximum, and cold downstream motion in zones where the liquid height has its minimum. The basic new feature in this streamline pattern is the coexistence of two convection rolls with different characteristic lengthscales. Thus in one spatial period of total wavelength l four convection cells are contained. The two different wavelengths of the streamline pattern are visible in the pattern of the solid–liquid interface. We shall term this type of pattern 'bimodal'. We should keep in mind, however, that the convective flow is not truly two-dimensional, as suggested by the roll pattern sketched in figure 9(*c*). From the corrugation of the interface we clearly see that the temperature field is three-dimensional since the interface represents an isothermal surface. However, from our experiments we cannot infer

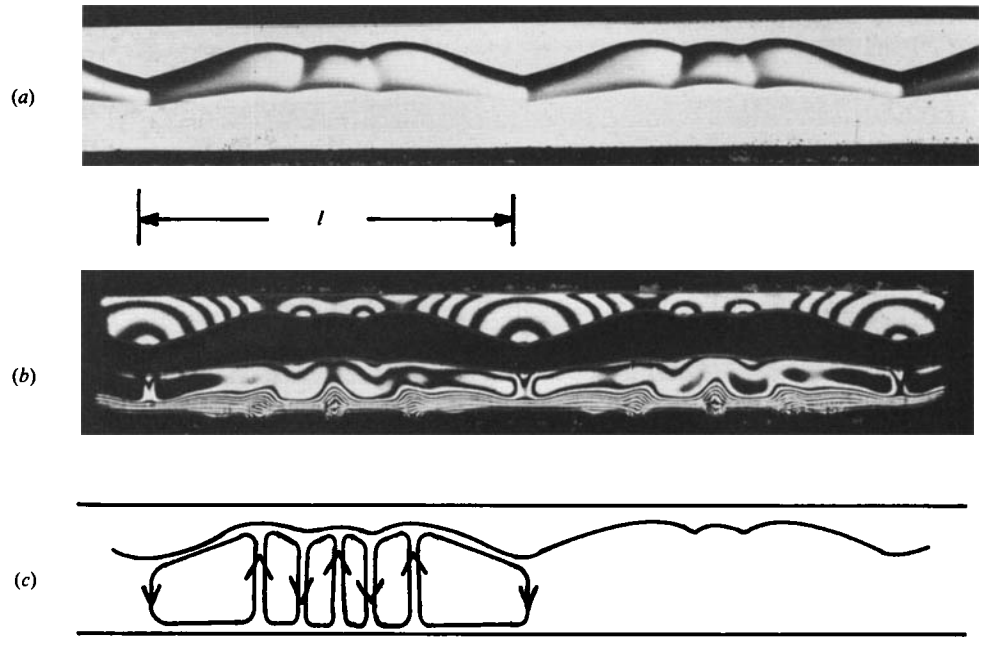

FIGURE 11. Bimodal pattern at $R = 16000$ and $A = 1.51$: (*a*) photograph; (*b*) differential interferogram of vertical beam splitting $e = 0.3$ mm; (*c*) streamlines.

what effect small but finite velocity components in the direction perpendicular to the optical plane have on the interfacial pattern.

For this bimodal roll pattern we find experimentally that, given the particular thermal boundary conditions, the lengthscales of the interfacial pattern are not unique (see figure 10). For the same Rayleigh number as in figure 9 the interfacial pattern is now characterized by a greater overall wavelength l. Both patterns, figures 9 and 10, proved to be stable during an observation time of more than 24 h. Whereas the pattern in figure 9 has been obtained by decreasing the liquid height, the pattern in figure 10 has been obtained by increasing the liquid height.

A different interfacial pattern with a still larger periodicity length l was observed at an even higher Rayleigh number. This pattern is displayed in figure 11 and seems to be characterized by three lengthscales. The interpretation of the interferogram in figure 11 (*b*) is similar to the previous cases. We identify four convection rolls with the same small lengthscale and two rolls with the same greater lengthscale; thus actually only two wavelength magnitudes occur. Therefore we also call the interfacial pattern of figure 11 'bimodal'.

Before we continue our report on pattern observation we shall suggest a plausible explanation for the occurrence of the bimodal patterns. The three bimodal patterns shown in figures 9, 10 and 11 all have in common that (i) there is a thermal boundary layer at the lower boundary of the liquid and (ii) there are two lengthscales that characterize the interfacial pattern. The instability of the liquid layer just beyond the critical Rayleigh number gives rise to a cellular flow characterized by one typical lengthscale, which correlates with the mean liquid height. At higher Rayleigh numbers thermal boundary layers develop near the lower and upper boundaries of the liquid layer. Now we utilize a model first described by Howard (1964). According to Howard the thermal boundary layers of thickness δ can become unstable at a

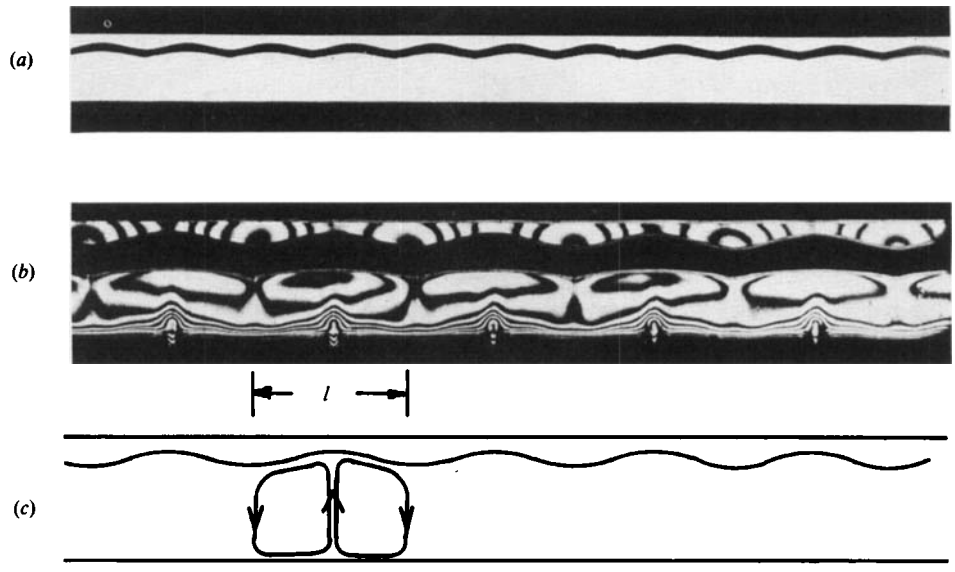

FIGURE 12. Roll pattern with wavenumber 4.3 at $R = 31000$ and $A = 1.0$: (*a*) photograph; (*b*) differential interferogram of vertical beam splitting $e = 0.3$ mm; (*c*) streamlines; note the change in scale from (*a*) to (*b*).

critical Rayleigh number of value between 1101 and 1708 (Chandrasekhar 1961). The critical thickness δ_c, where the temperature boundary layer is exactly critical, is given by the relation

$$\delta_c = \left(R_c \frac{\nu \kappa^{(L)}}{\frac{1}{2} g \alpha (T_0 - T_s)} \right)^{\frac{1}{3}} \quad (1101 \leqslant R_c \leqslant 1708). \tag{3.1}$$

Using the material constants and the temperature difference $T_0 - T_s$ from our experiment, the value of δ_c is obtained within the bounds of 2.1 mm $\leqslant \delta_c \leqslant$ 2.4 mm. We conclude that the wavelength that originates from an instability of the thermal boundary layer should be of about the same magnitude as δ_c. And indeed the small lengthscale that one recognizes in the bimodal interfacial patterns is 2.5 ± 0.5 mm. Moreover, the small lengthscale in the interface has been observed to be approximately constant and equal for all bimodal patterns in all the experiments. This is due to the fact that all parameters which appear in (3.1), in particular the temperature difference $T_0 - T_s$, were constant in the experiments so that δ_c is constant under these conditions.

The fact that a thermal boundary-layer instability causes a second lengthscale to occur is well known in the Bénard problem (Busse & Whitehead 1971). In that case the so-called bimodal convection is observed as a three-dimensional form of stationary convection for Rayleigh numbers greater than 23000. We note here that, contrary to those findings, quasi-two-dimensional bimodal patterns are observed in our experiments since three-dimensional effects are suppressed by the lateral walls.

After these explanations concerning the bimodal pattern we continue our report on pattern observation. At the particular Rayleigh number $R = 31000$ the bimodal pattern is replaced by a mono-modal pattern with a smaller wavelength. The corresponding wavenumber is $k = 4.3$. A typical situation is given by figure 12. This is a steady state but it proved to have a transitional character, since we find at lower

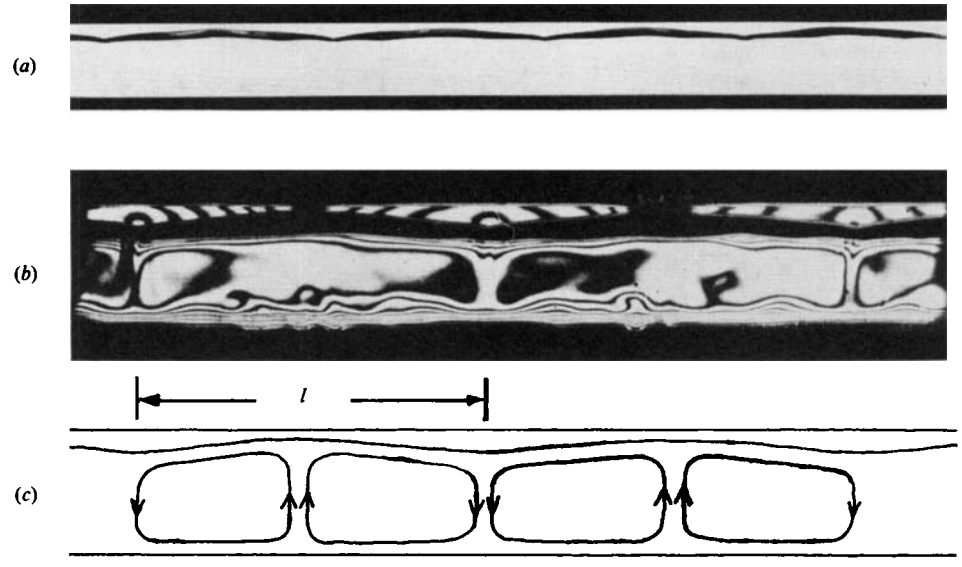

FIGURE 13. Roll pattern with unsteady motion in the thermal boundary layer at the lower bound of the liquid at $R = 41000$ and $A = 0.83$: (*a*) photograph; (*b*) differential interferogram of vertical beam splitting $e = 0.3$ mm; (*c*) streamlines; note the change in scale from (*a*) to (*b*).

Rayleigh numbers steady-state 'bimodal patterns' whereas at higher Rayleigh numbers we find fluctuating unsteady motion in the liquid layer. More specifically, at a Rayleigh number one measuring point beyond that in figure 12, the interfacial pattern shown in figure 13 appeared. The wavelength of the spatial periodicity of the interface is much larger than that in figure 12(*a*). The interferogram of figure 13(*b*) shows a distinct boundary-layer character in the temperature distribution. Furthermore the fringes along the lower boundary were seen to pulsate slightly up and down while the fringes near the liquid–solid interface were stationary. The typical time constant of the pulsations is of the order of 20 s. Assuming that the pulsations of the lower thermal boundary layer are caused by a thermal instability, the value of the thermal-diffusion time can be calculated based on the above-derived critical boundary-layer thickness δ_c. The calculated values are between 49 s and 65 s, which means that the diffusion time is of the same order as the typical time constant that was measured from the fringe-pattern fluctuations of the real-time interferograms using a stopwatch. The steady state of the thermal boundary layer at the upper end of the liquid region is ascribed to the influence of the latent heat of fusion, which in any transient process has to be transferred near the interface and therefore is supposed to have a retarding effect on all transient processes at the interface. The wavelength of the structure of the fluid motion is large compared to the mean liquid-layer height in this case.

At an even higher Rayleigh number of about 170000 and $A = 0.14$, the thermal boundary layer at the upper boundary of the liquid phase becomes unsteady. This is attributed to the fact that in this case the solid layer was very thin (i.e. some tenths of a millimetre thick) so that the liquid was nearly in direct contact with the copper.

We have so far described the various interfacial and fluid-flow patterns observed for fully developed convection. In the following section we shall arrange the different phenomena in a stability chart.

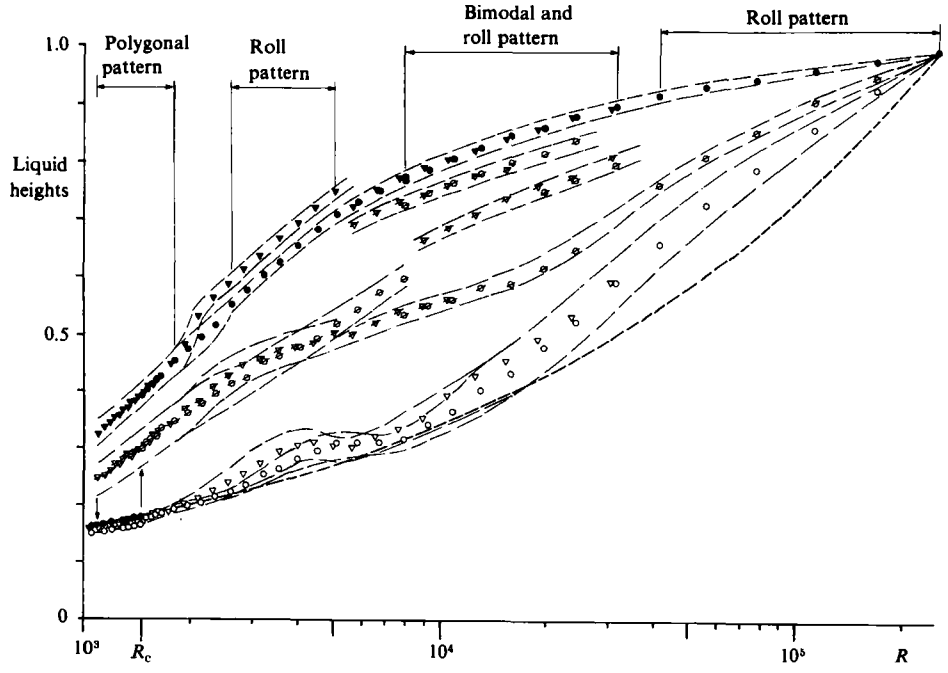

FIGURE 14. Normalized liquid heights depending upon the Rayleigh number: ●, ▼, local maxima of the liquid height; ∅, ∇̸, local minima of the liquid height; ○, ▽, liquid heights at the vertical Plexiglas boundaries; circles ●, ∅, ○ (triangles ▼, ∇̸, ▽) indicate measuring points which were obtained after an increase (decrease) in the Rayleigh number; ---, heat-conduction height; = =, scatter.

3.3. *Stability chart of interfacial patterns*

We shall next describe the different interfacial patterns by evaluating their particular wavenumbers. The wavenumber is based on the mean liquid height, i.e. the arithmetic-mean value of the local maxima and minima of the liquid heights (see (2.3)).

In figure 14 the normalized heights h_m/h and h_M/h are plotted versus the Rayleigh number. By varying the upper boundary temperature T_1 the height h_L/h was varied in the range $0.16 \leqslant h_L/h \leqslant 1$. The liquid heights at the vertical Plexiglas boundaries were approximately equal to h_L throughout the experiment. This is explained by the fact that the heat is transferred by conduction in the vertical boundaries and also in the viscous boundary layers close to them.

Next we mention some particular features of h_M and h_m in certain ranges of the Rayleigh number. Near the critical Rayleigh number R_c we find the hysteresis loop for h_M and h_m. In the range $2600 \leqslant R \leqslant 5000$ roll patterns occur. Here h_M depends upon the way in which the steady-state boundary conditions are established. If the particular value of the Rayleigh number is approached from lower values, h_M is lower than if this value of the Rayleigh number is approached from above. The relative corrugation of the interface $(h_M - h_m)/\frac{1}{2}(h_M + h_m)$ varies between 30 and 40 % in the range of roll patterns.

In the range of Rayleigh numbers $8000 \leqslant R \leqslant 32000$, which is marked in figure 14 as bimodal and roll pattern, all maxima of the liquid height fall within the same margin. This is independent of the way by which the corresponding boundary conditions are established and is also independent of the interfacial pattern. However,

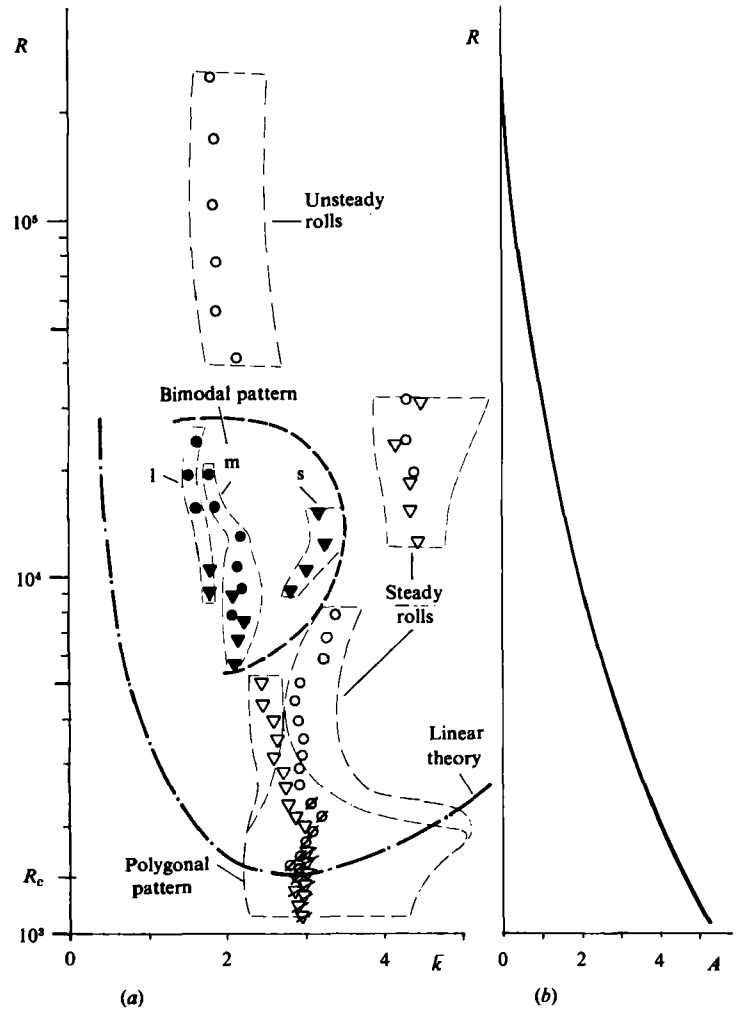

FIGURE 15. Stability chart for interfacial patterns; ∅, ⊘, polygonal pattern; ○, ▽, roll pattern; ●, ▼, bimodal pattern with --- the corresponding stability boundary, l, m and s indicate long, middle and short bimodal patterns; circles ●, ∅, ○ (triangles ▼, ⊘, ▽) indicate measuring points which were obtained after an increase (decrease) in the Rayleigh number; —·—, linear theory; = =, scatter.

we found in our experiments that for the same external boundary conditions three different values of the minima of the liquid height can occur. This is indicated in figure 14 by the chains of crossed symbols. The pattern in figure 9 corresponds to the upper and the middle chain of symbols, the patterns in figures 10 and 11 to the upper and lower chain, and the pattern in figure 12 only to the middle chain of symbols.

The various flow and interfacial patterns can be arranged in a Rayleigh-number and wavenumber graph by making use of the above-discussed liquid heights. This has been done in figure 15. The different patterns are characterized by their individual periodicity lengthscale l, which we previously termed wavelength. A dimensionless mean wavenumber $\bar{k}$ is defined according to (2.3) using the horizontally averaged liquid height $\bar{h}_L$ and the mean value of the spatial periodicity length $\bar{l}$. We also consider a local wavenumber k_i by using the local values l_i and the corresponding

local mean liquid height $\frac{1}{2}(h_M + h_m)_i$ in the wavenumber relation (2.3). The values of k_i scatter around the mean value $\bar{k}$. In figure 15(*a*) the band of scattering values k_i is indicated by the dashed light lines.

Figure 15 displays the conditions for the occurrence of the different patterns, where both the symbols in the $(R, \bar{k})$-graph and the corresponding value on the solid curve in the (R, A) graph define the particular experimental state. We mention here that our experiments cover only one particular section in the generally three-dimensional manifold of parameters R, A, $\bar{k}$. This is so because during the experiments only the temperature T_1 at the upper boundary of the layer was varied.

The dash-dotted line in figure 15(*a*) is the curve of marginal stability for the onset of convection in the liquid phase. The curve was calculated by a linear stability theory outlined in DMD. The calculated critical Rayleigh number $R_c = 1493$ and wavenumber $k_c = 2.82$ are in good agreement with the experimental values $R_c = 1450$ and $\bar{k}_c = 2.9$. The subcritical states related to a polygonal, three-dimensional pattern are found below the curve of marginal stability. In the Rayleigh-number range $1080 < R < 2600$, where polygonal patterns were observed, a large scatter in the local wavenumber exists. This scatter is mainly attributed to sidewall effects, which prevent the formation of the regular hexagonal pattern observed in an infinitely extended horizontal layer (see DMD). For Rayleigh numbers beyond $R = 2600$ we find roll patterns. Since this pattern is more appropriate to the narrow-spaced test volume the periodicity of the pattern is more regular, which results in a smaller experimental scatter of the local wavenumber.

The transitions from polygonal to roll pattern and the reverse exhibit a hysteresis loop in a small range of Rayleigh numbers centred around $R = 2300$. Furthermore, the wavenumbers of the roll pattern appearing in experiments with decreasing Rayleigh numbers are smaller than those obtained from experiments with increasing R (see also figure 8). Roll patterns were also found experimentally in the Rayleigh-number ranges $1.3 \times 10^4 < R < 3.2 \times 10^4$ and $4 \times 10^4 < R < 2.5 \times 10^5$. While the roll convection related to the first range and to wavenumbers of about $\bar{k} = 4.3$ is at steady state, the convective motion in the second range is a fluctuating one with wavenumbers k of about 2. The transition from steady-state flow to unsteady motion occurred in the experiment when the Rayleigh number was increased from $R = 3.1 \times 10^4$ to $R = 4.1 \times 10^4$. Typical interfacial patterns related to the first and second range can be seen in figures 12 and 13.

In figure 15(*a*) the parameter domain of the bimodal patterns is bounded by the dashed heavy line. The bimodal patterns of short, medium-sized, and long periodicity lengthscale are marked in the graph by s, m and l respectively. The 'short' bimodal pattern was only observed when R was decreased quasi-steadily, whereas the other two occurred after increasing or decreasing R monotonically and quasi-steadily. Typical interfacial patterns belonging to the different types of bimodal patterns can be seen in the photos of figures 9, 10 and 11. Furthermore, from our experiments we found some indication that the overall wavelengths l of the various bimodal and roll patterns are interrelated. They can be transformed into one another by adding or subtracting multiples of the small boundary-layer lengthscale of the bimodal patterns. However, further work is necessary to clarify this indication (for more details see Dietsche 1984).

4. Summary

In this paper we have examined a narrow horizontal layer of a single-component liquid (cyclohexane), which is heated from below and cooled to freezing from above. We have outlined an experiment with values of A between 4 and 5, in which a strong hysteresis behaviour of the steady-state liquid height is observed at the onset and disappearance of convection. The liquid height undergoes jump transitions and thereby varies by a factor of more than 2. The steady-state convection still occurs at Rayleigh numbers which are up to 25% subcritical. The hysteresis and jump phenomena are interpreted by means of a weakly nonlinear analysis of Davis, Müller & Dietsche (1984), for a horizontally infinite layer. We have discussed the influence of the lateral walls on the interfacial pattern. We report a pattern transition at the solid–liquid interface from a 'polygonal' to a 'roll pattern', which occurs when the ratio of the mean liquid-layer height to the layer depth exceeds the value of about 1:4. We have described and explained 'bimodal' interfacial patterns. These are characterized by the coexistence of two different wavelengths and are shown to be related to a thermal-boundary-layer instability. The various interfacial patterns are displayed in the form of a stability chart.

The authors gratefully acknowledge the stimulating discussions with Prof. S. H. Davis during the preparation of this article.

REFERENCES

BUSSE, F. H. & WHITEHEAD, J. A. 1971 Instabilities of convection rolls in a high Prandtl number fluid. *J. Fluid Mech.* **47**, 305–320.

CAREY, V. P. & GEBHART, B. 1982 Transport near a vertical ice surface melting in saline water: experiments at low salinities. *J. Fluid Mech.* **117**, 403–423.

CHALMERS, B. 1964 *Principles of Solidification.* Wiley.

CHANDRASEKHAR, S. 1961 *Hydrodynamic and Hydromagnetic Stability.* Clarendon.

DAVIS, S. H. 1967 Convection in a box: linear theory. *J. Fluid Mech.* **30**, 465–478.

DAVIS, S. H., MÜLLER, U. & DIETSCHE, C. 1984 Pattern selection in single-component systems coupling Bénard convection and solidification. *J. Fluid Mech.* **144**, 133–157.

DIAZ, L. A. & VISKANTA, R. 1984 Visualization of the solid–liquid interface morphology formed by natural convection during melting of a solid from below. *Intl Comm. Heat Mass Transfer* **11**, 35–43.

DIETSCHE, C. 1984 Einfluß der Bénard-Konvektion auf Gefrierflächen. Dissertation, Universität Karlsruhe, West Germany (*KfK-Rep.* 3724).

FARHADIEH, R. & TANKIN, R. S. 1975 A study of the freezing of sea water. *J. Fluid Mech.* **71**, 293–304.

FRICK, H. & CLEVER, R. M. 1980 Einfluß der Seitenwände auf das Einsetzen der Konvektion in einer horizontalen Flüssigkeitsschicht. *Z. angew. Math. Phys.* **31**, 502–513.

HAUF, W. & GRIGULL, U. 1970 Optical methods in heat transfer. *Adv. Heat Transfer* **6**, 133–366.

HOWARD, L. N. 1964 Convection at high Rayleigh number. In *Proc. 11th Intl Congr. of Applied Mechanics, München* (ed. H. Görtler), pp. 1109–1115. Springer.

HUPPERT, H. E. & TURNER, J. S. 1978 On melting icebergs. *Nature* **271**, 46–48.

JAKEMAN, E. & HURLE, D. T. J. 1972 Thermal oscillations and their effect on solidification processes. *Rev. Phys. Tech.* **3**, 3–30.

KOSTER, J. N. 1983 Interferometric investigation of convection in plexiglas boxes. *Exp. Fluids* **1**, 121–128.

MARSHALL, R. & DIETSCHE, C. 1982 Comparison of paraffin wax storage subsystem models using liquid heat transfer media. *Solar Energy* **29**, 503–511.

MÜLLER, G., SCHMIDT, E. & KYR, P. 1980 Investigation of convection in melts and crystal growth under large inertial accelerations. *J. Cryst. Growth* **49**, 387–395.

OERTEL, H. & BÜHLER, K. 1978 A special differential interferometer used for heat convection investigations. *Intl J. Heat Mass Transfer* **21**, 1111–1115.

SAITOH, T. & HIROSE, K. 1982 High Rayleigh number solutions to problems of latent heat thermal energy storage in a horizontal cylinder capsule. *Trans. ASME* C: *J. Heat Transfer* **104**, 545–553.

STORK, K. & MÜLLER, U. 1972 Convection in boxes: experiments. *J. Fluid Mech.* **54**, 599–611.

TURNER, W. D. & SIMAN-TOV, M. 1971 Heating 3 – An IBM 360 heat conduction program. *ORNL-TM*-3208.